

Unsupervised Domain Adaptation through Iterative Consensus Shift in a Multi-Task Graph

Emanuela Haller^{*1,2,4}, Elena Burceanu^{*1,3,4}, and Marius Leordeanu^{1,2,4}

¹Bitdefender

²University Politehnica of Bucharest, Romania

³University of Bucharest, Romania

⁴Institute of Mathematics of the Romanian Academy, Romania

haller.emanuela@gmail.com, eburceanu@bitdefender.com, leordeanu@gmail.com

Abstract

Babies learn with very little supervision by observing the surrounding world. They synchronize the feedback from all their senses and learn to maintain consistency and stability among their internal states. Such observations inspired recent works in multi-task and multi-modal learning, but existing methods rely on expensive manual supervision. In contrast, our proposed multi-task graph, with consensus shift learning, relies only on pseudo-labels provided by expert models. In our graph, every node represents a task, and every edge learns to transform one input node into another. Once initialized, the graph learns by itself on virtually any novel target domain. An adaptive selection mechanism finds consensus among multiple paths reaching a given node and establishes the pseudo-ground truth at that node. Such pseudo-labels, given by ensemble pathways in the graph, are used during the next learning iteration when single edges distill this distributed knowledge. We validate our key contributions experimentally and demonstrate strong performance on the Replica dataset, superior to the very few published methods on multi-task learning with minimal supervision.

1. Introduction

Seeing the world from multiple perspectives and with different interpretations offers an invaluable source of information, as shown by works using various features extractors [2, 15, 9, 37] or multiple supervised tasks [12, 39]. While the multi-tasks approaches attain a more comprehensive and fundamentally better understanding of the visual scene than the single-task ones, they require a larger amount of labeled data for the same input.

Our proposal for satisfying the unlabeled data problem, different from current multi-modal [23, 22] and multi-task-graph approaches [14, 38], is to take advantage of the existing pre-trained experts, on many different tasks in the state-of-the-art literature and offer a principled way to learn unsupervised on novel target domains, by using their selective consensual knowledge within a graph neural structure. Each node in our graph represents a specific interpretation or task. Each graph edge is a neural net that transforms one task into another. Pseudo labels for a given task are obtained by combining all pathways' outputs reaching the corresponding node. Very different from the recent NGC model [14]), we connect all tasks with neural networks and do not need any labeled data on the target domain. The experts we start with can be pre-trained independently on any, potentially very different, datasets. Also, different from the recent [14, 38], we show that an intelligent consensus-finding selection procedure is required to create strong pseudo-labels from many unsupervised pathways that could lead to a significant improvement over the initial experts. The unsupervised, consensus-based learning process continues for several iterations of the graph, with experimentally provable improvements from one iteration to the next. Our **key contributions** that are theoretical, as well as experimental, are:

1. **We introduce iterative Consensus Shift (CShift)**, an algorithm for unsupervised multi-task learning on novel target domains, applied to neural graph models. CShift exploits, using an intelligent selection procedure, the consensual agreements among multiple graph pathways, where each path transforms differently an input task into another. These ensembles of pathways become powerful unsupervised teachers in the multi-task graph, on novel target domains. The learning process continues over multiple graph iterations. After each iteration the pseudo-labels at every node, given by the consen-

^{*}Equal contribution

	Supervision on target domain	Uses ensembles	Ensemble as supervision signal	Selection based ensemble	Unsupervised domain adaptation	Fully-connected graph
XTC [38]	supervised	✗	N/A	N/A	✗	✓
NGC [14]	semi-supervised	✓	✓	✗	✗	✗
CShift (ours)	unsupervised	✓	✓	✓	✓	✓

Table 1. Main differences between our CShift algorithm and state-of-the-art methods for learning in Multi-Task Graphs.

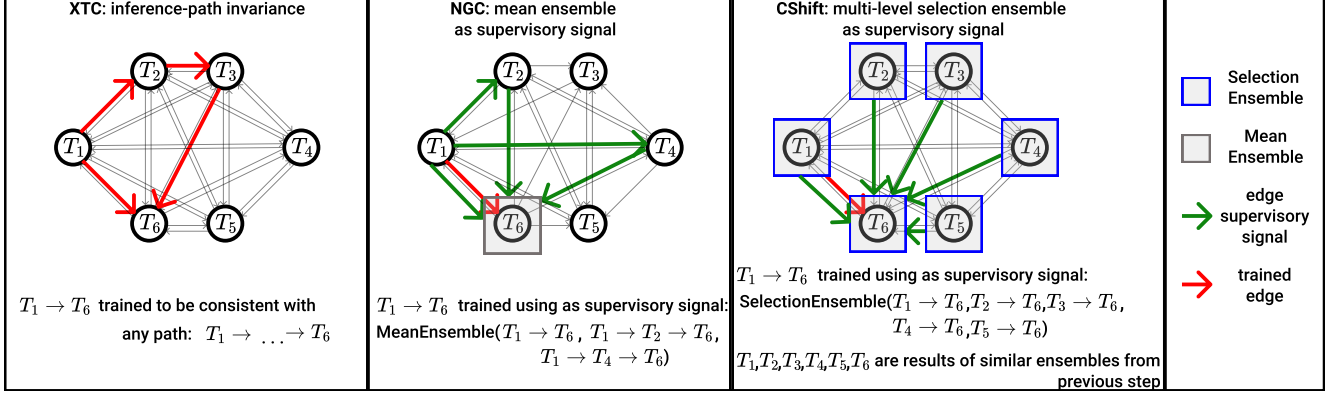


Figure 1. Illustration of the different training strategies employed by Multi-Task Graph methods in comparison to our approach (CShift).

sual output at that node, shift, thus departing from and improving over the initial experts.

2. **We show in extensive experiments** on a recent multi-task dataset that CShift learns unsupervised to self-improve, over multiple tasks, from one iteration to the next, while also significantly outperforming the state-of-the-art experts used to generate the first pseudo-labels.

1.1. Relation to prior work

Relation to Ensembles and Experts. The idea of different paths working together to reach a common goal was frequently demonstrated [25] over time. Our solution is related to the idea of guiding the learning process using a set of expert models, an approach that proved effective for instance for tasks like video and image retrieval [5, 15, 19, 21].

Relation to Unsupervised Representation Learning. Recent formulations use pretext tasks [7, 42, 20, 41], clustering [3, 40, 31], minimize contrastive noise [10, 18, 30] or are based on generative adversarial models [4]. Different from these methods, we use as pseudo-ground truth the consensual output over multiple paths reaching the same task.

Relation to Multi-Modal Learning. Several recent works combine modalities and tasks. Different from the method in [23], using multiple modalities for predicting multiple tasks, we rely on the complex interactions between tasks’ output domains, modeled as a bidirectional graph.

Different from GDT [22] or GDT-related methods using multi-modal data transformation as self-supervision [29, 18], we learn complex interactions between tasks without ground truth, relying only on consensus and selection as supervision.

Relation to Multi-Task Learning. [39] studies the underlying connections between different tasks and proves that such relations can be exploited to effectively reduce the labeled data required for training. Different from XTC [38], we assume no multi-task annotated data on the target domain and rely solely on per-task expert models, pre-trained on different domains to provide the initial pseudo-labels. Moreover, the consensus shift method learns completely unsupervised on the target domain, relying solely on selection and consensus over multiple pathways reaching a given task node, over multiple graph iterations.

From the architectural point of view, our model is related to the recently proposed Neural Graph Consensus (NGC) model [14], which also connects multiple interpretations and tasks into a single graph of neural networks. NGC is based on a semi-supervised training, initializing the model in a supervised fashion, using ground truth labels from the same target domain. Our model strongly differs from NGC by four essential contributions: **1)** we show that an intelligent selection mechanism over the ensembles of pathways reaching a node produces significantly better results than the simple mean ensemble presented in NGC; **2)** we also propose a multi-level ensemble mechanism, as the ensemble results associated to one node are considered as both supervisory

signal for that node and as input signals for all out-edges. This idea gives better results since ensembles always provide superior results to single links, a fact that was insufficiently exploited in NGC. **3)** CShift is initialized with pseudo-labels generated by out-of-domain experts, while NGC assumes a fully supervised initialization step. **4)** Our neural graph model is fully connected and proves to be significantly more robust than NGC, once our selection procedure for finding consensus is applied.

In Tab. 1 and Fig. 1 we summarize the main differences between CShift and the recent XTC [38] and NGC [14].

2. Our Approach

We propose a novel Multi-Task Graph (Fig. 2-b) and the learning CShift algorithm, which uses as supervision the consensual output, extracted through an intelligent selection procedure, over multiple graph pathways that reach a given node. As mentioned previously, each node in the graph represents a task, a view, or an interpretation of the world. Each edge is a neural net that transforms one task at one node into another, from a different node. Our graph is directed and fully connected. In Fig. 2 we illustrate the main steps of our approach. All edges of our graph are initially trained using pseudo-labels for nodes, generated by out-of-domain experts. After initializing the edges (Fig. 2-a), we introduce **the view associated with a node**, computed as the ensemble result of all the node’s in-edges. These views will become the pseudo-ground truth labels, during the subsequent learning iterations in the graph and constitute a major difference between our model and both the recent XTC and NGC models. The views (pseudo-labels), will shift from one learning iteration to the next, using the CShift learning algorithm, described next in more detail. CShift uses the views at each node, transmits information through the out-edges towards other nodes, and also collects the information from the in-edges, in order to create the new views, at the next iteration, by a selection mechanism that establishes the consensus over the multiple incoming edges. The process is repeated in principle until an equilibrium is found, at convergence. It should be clear at this point that the iterative graph learning phase is unsupervised and that the initial experts used could be created completely independently, using information from other datasets and domains, as our experiments will show. In Fig. 2-c we present a visual scheme of CShift, while in Alg. 1 we state its main formalized steps.

2.1. Multi-Task Graph

We formally define the Multi-Task Graph over a set T of t tasks (e.g. semantic segmentation, single-image depth estimation, surface normals - Sec. 3), each illustrating a different view of the scene. There are one-to-one correspondences between graph nodes and the set of tasks, and each edge is an encoder-decoder neural net transformation between source

Algorithm 1 - CShift: Multi-Task Graph Learning with Consensus Shift

X_i - data sample i ; T - a set of tasks;
 Exp_d - expert for task d ; $e_{s \rightarrow d}$ - edge from task s to task d

```

// Get  $m$  splits of data samples from the target domain
1:  $D_j = \{X_i | i \in \overline{1, m_j}\} \forall j \in \overline{1, m}$ 
// Use experts to generate the initial pseudo-labels
2:  $Y_{i;d} \leftarrow \text{Exp}_d(X_i) \forall d \in T, i \in \overline{1, m_j}, j \in \overline{1, m}$ 
3: for  $k \leftarrow 1$  to  $m$  do
    // Update views - enable multi-level ensembles
4:    $X_{i;d} \leftarrow Y_{i,d}, \forall i \in \overline{1, m_j}, j \in \overline{1, m}, d \in T$ 
    // Learn from pseudo-labels
5:   train  $e_{s \rightarrow d} \forall s, d \in T$ 
      with samples  $\{(X_{i;s}, X_{i;d}) | X_i \in \cup_{j=1}^k D_j\}$ 
    // Generate new pseudo-labels
6:    $\mathcal{N}(X_{i;d}) \leftarrow \{e_{s \rightarrow d}(X_{i;s}) | s \in T\}$ 
7:    $Y_{i;d} \leftarrow \text{ConsensusShift}(\mathcal{N}(X_{i;d}))$ 
8: end for

```

and target task nodes (Fig. 2-b). Consequently, our graph $G = (T, E)$ with $E = \{e_{s \rightarrow d} | e_{s \rightarrow d}(X_s) = X_d, s, d \in T, s \neq d\}$, where X_s is the scene representation under task s , and $e_{s \rightarrow d}$ is the neural network transforming the view between source task s and destination task d . The graph edges are initialized as mentioned previously and explained in more detail next, using expert teachers (pre-trained out-of-domain), one per considered task. For the target domain, we only receive a set of raw rgb images.

Passing an rgb image through the graph: given a raw rgb frame, we associate it to the rgb node. Next, we will enforce and exploit a fundamental property of the graph: the consensual representation. The idea is that no matter what pathway the image will take through the graph, being transformed from one node (task) to the next, once it reaches a given node (task), it should ideally have the same representation as the one obtained by taking any other pathway reaching the same node. In other words, all pathways ending at a given node in the graph should have the same output.

Initializing the graph. Other approaches [14, 38] start with a supervised training phase of all the out-edges of the rgb node $\{e_{rgb \rightarrow d} | \forall d \in T\}$, requiring multi-task annotated datasets. As we work in the unsupervised regime for the target domain, our initial views (pseudo-labels) for different tasks are obtained from a set of out-of-distribution expert models (Fig. 2-a). We define a set of t experts $\{\text{Exp}_d | \forall d \in T\}$, each associated to one of our nodes (tasks) (Sec. 3). Then the initial edges are learned by distilling the pseudo-labels given by the experts.

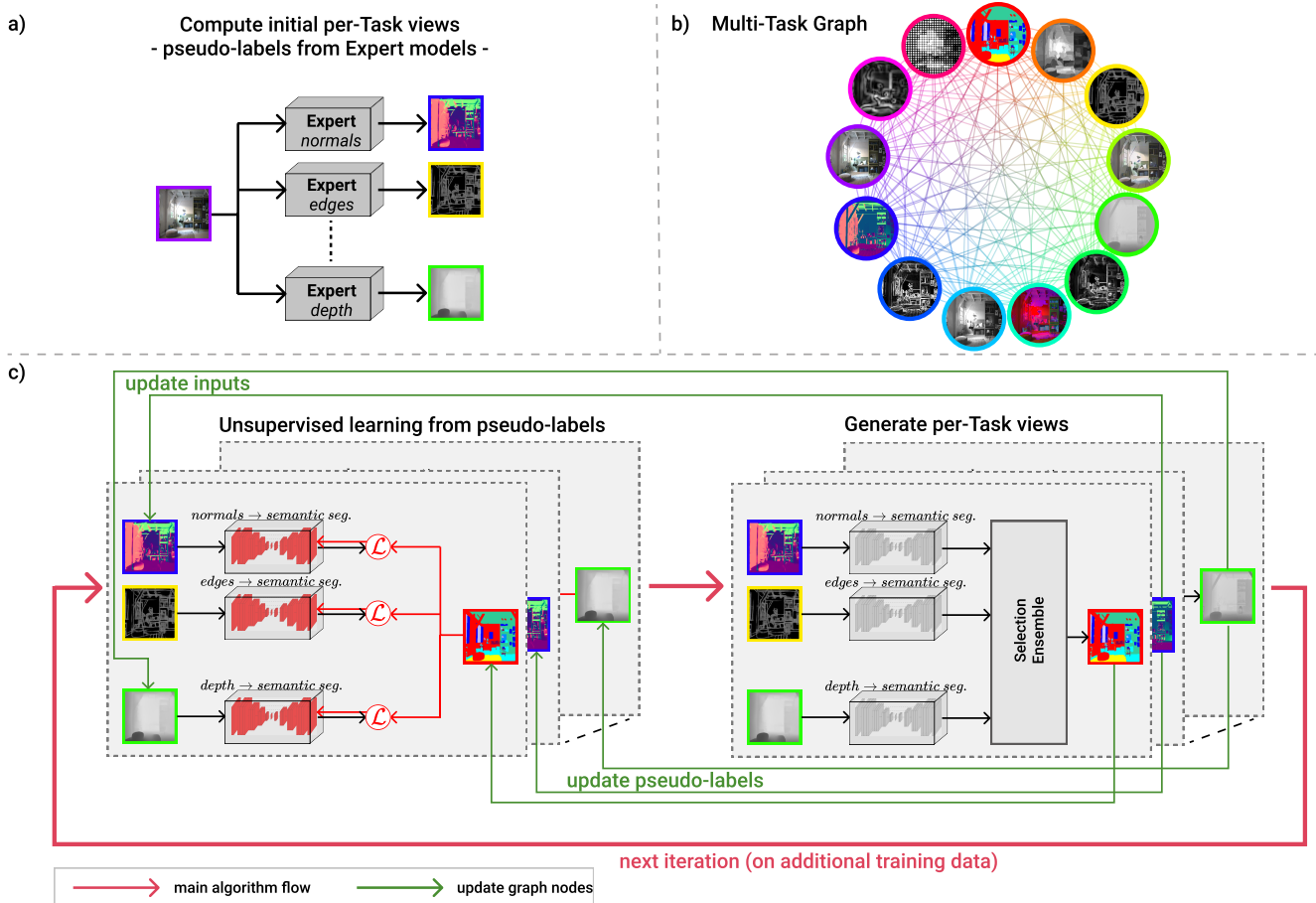


Figure 2. Main architectural elements of our Consensus Shift (CShift) system. **a)** Initialization from expert models. Based on the *rgb* image, the experts (which are considered as black boxes in our system) predict the initial pseudo-labels for each considered task. We emphasize that the experts are trained on different distributions than our target domain. **b)** Illustration of the fully-connected Multi-Task Graph, with 13 nodes corresponding to the 13 considered tasks. The edges are transformations between their source and destination tasks/nodes. **c)** The iterative process of CShift. Given the pseudo-labels for all tasks, we train each graph edge. Further, for each node, we compute its new pseudo-labels as the consensual representation of its in-edges, through the selection ensemble mechanism. The newly computed labels of a node become its supervisory signal in the next iteration. They also become inputs for all the out-edges of the node.

2.2. Consensus Shift Learning

Next, we present CShift learning (Alg. 1) in more detail. As discussed, consensus between several edges reaching a given node could provide a more reliable view of that node. With each learning iteration, the views (pseudo-labels) will shift, departing and potentially improving from the initial pseudo-labels from experts. At each such learning phase, the nodes' views are used to train the single edges connecting them and thus distill the distributed graph knowledge from the previous learning phase.

Given a destination node d , all edges reaching this node $\{e_{s \rightarrow d} | s \in T, s \neq d\}$ are transformations of the source tasks $\{s | s \in T\}$. Each transformation is, in fact, the last step of a longer graph path, starting in the *rgb* node and ending in node d . All paths should ideally be in consensual agreement,

but in practice, when they are not, an intelligent mechanism is needed to extract the common, robust knowledge shared by their majority or the most important cluster. We employ the discovery of consensus, among multiple outputs from incoming edges, at the pixel level.

Considering the destination node d and a sample X_i , CShift updates the sample's view, associated with task d , $X_{i;d}$. For simplicity, we consider that task d has a single-map output (e.g. depth map), but multi-channel tasks are treated similarly. We define the neighbourhood of a sample X_i under a task d as the set of all transformations of different views of the sample i , towards the destination task, joined with the current pseudo-label of the destination task:

$$\mathcal{N}(X_{i;d}) = \{e_{s \rightarrow d}(X_{i;s}) | \forall s \in T\} \cup \{X_{i;d}\}. \quad (1)$$

The consensual representation is computed as a function f

gathering information from all the neighbours of $X_{i;d}$, parameterized by the weights $\mathbf{W}_{i;d} \in \mathbb{R}^{h \times w \times t}$ (where (h, w) is the image size):

$$X_{i;d} = f(\mathcal{N}(X_{i;d}); \mathbf{W}_{i;d}) \quad (2)$$

The per-pixel weights capture the consensus between the different predictions. \mathbf{W} has a channel associated with each task node, which indicates the similarity of the corresponding prediction with the current representation of the destination task. The algorithm aims to identify the areas of the prediction maps that are perceptually similar and push them further in the ensemble while downgrading regions that seem to be noisy and uncorrelated with the other predictions. For a location (x, y) and a given task s , the weights are computed as follows:

$$\mathbf{W}_{i;d}[x, y, s] = \frac{K(\text{dist}(X_{i;s}, X_{i;d})[x, y])}{\sum_{Z \in \mathcal{N}(X_{i;d})} K(\text{dist}(Z, X_{i;d})[x, y])}, \quad (3)$$

where $\text{dist} : \mathbb{R}^{h \times w} \rightarrow \mathbb{R}^{h \times w}$ is a distance function capturing the similarity between two different prediction maps and $K : \mathbb{R} \rightarrow \mathbb{R}$ is the kernel function that determines the weight of nearby points. The proposed methodology is an intelligent selection ensemble that can automatically select the most representative consensual representation of the in-edges. Our experiments (Sec. 3.1) prove that the selection strategy is robust to noisy connections. The adaptive per-pixel weighting allows CShift to keep the most relevant information from all the input maps, even when some maps are less reliable.

2.3. Unsupervised Domain Adaptation

CShift requires no human-annotated data for the target domain. We take advantage of existing state-of-the-art expert models that distill research years and valuable expertise and provide reliable pseudo-labels for each of the considered tasks. When applied to novel domains, the weakness of these experts is that they are trained on different, out-of-domain distributions. We first transfer their knowledge in our graph edges. Then our learning method, by exploiting and enforcing the overall consensus among all tasks, allows the graph to adapt by itself to the target domain, thus overcoming the domain gap, as shown in our tests (Sec. 3.2 and Sec. 3.3). To emphasize the domain adaptation capabilities of CShift, we employ the Maximum Mean Discrepancy [8] (MMD) method for measuring the domain dissimilarity between our target domain and the expert source domains. MMD is a strong and widely used [13, 16, 35] non-parametric metric for comparing the distributions of two datasets. We follow the methodology in [8] and compute the unbiased empirical estimate of squared MMD. Our experiments show (Sec. 3.2) that there is a large distributional shift between our target domain and the domains of the original expert models. This

result, along with the results in Sec. 3 prove the unsupervised domain adaptation capabilities of our method.

3. Experimental Analysis

Dataset. We perform experiments on Replica [28], a dataset of photo-realistic 3D indoor scenes, comprising 18 scenes, with a total of 48 rooms. In practice, we consider two iterations for training our Multi-Task Graph and use two unsupervised train sets (9600+9600 samples), two validation sets (960+960 samples), and a test set of 960 samples (never seen during the unsupervised learning process). During training and validation, only the raw *rgb* images are available. Ground truth is used only for evaluation on the test set.

Expert Models. We employ per-task expert models, with input *rgb* only, trained on out-of-domain data, to initialize the per-node pseudo-labels (Fig. 2-a). Conceptually, in the first learning iteration, the experts replace the direct edges starting from the *rgb* node. Then, the computed views of a node become supervisory signals for the in-edges of that node and inputs for the out-edges (e.g. for training edge $e_{\text{depth} \rightarrow \text{halftone}}$, the depth input is obtained by applying the depth expert over the *rgb* frame and the halftone pseudo-label by extracting the halftone from *rgb*.)

Our graph contains a total of 13 task nodes, including the *rgb* one, thus we consider 12 experts ranging from trivial color-space transformations to heavily trained deep nets: 1) halftone computed using *python-halftone*; 2) grayscale and 3) hsv computed with direct color-space transformations; 4) depth and 5) surface normals obtained from the XTC [38] experts; 6, 7, 8) small, medium and large scale edges extracted using a Sobel-Feldman filter [6], and more complex 9) edges extracted using the DexiNed [26] expert; 10) super-pixel maps extracted using SpixelNet [36]; 11) cartoonization got from WBCartoon [33] and 12) semantic segmentation maps computed with HRNet [32]. The deep nets expert models are trained on a large variety of datasets: 4) and 5) Taskonomy [39], 9) BIPED [27], 10) SceneFlow [17] + BSDS500 [1], 11) FFHQ [11], 12) ADE20k [44]. Note that these datasets are built for a different purpose and has a different distribution than our domain.

We evaluate our model on two tasks: depth and surface normals predictions from *rgb*. The XTC experts' output on *depth* and *normals* tasks are not aligned with annotations from Replica as their original datasets use different conventions. Thus, on *depth*, following the methodology of self-supervised methods [45], we performed a histogram specification alignment between expert results and ground truth annotations. On *normals*, we removed the 3rd channel in the XTC expert according to Replica, which has normals with only 2 independent channels.

Method	<i>depth</i>	<i>normals</i>	<i>rgb</i>
Expert [38]	14.58	8.30	-
Mean Ensemble [14]	12.94	7.95	4.30
CShift w/ Variance	12.80	7.91	2.12
CShift w/ PSNR	12.89	8.12	4.25
CShift w/ SSIM	12.80	7.89	2.38
CShift w/ L1	12.81	7.73	2.16
CShift w/ L2	12.79	7.72	2.45
CShift w/ LPIPS	12.77	7.61	2.06

Table 2. Ablation study on different distance metrics on Replica dataset, for the first iteration. In all considered configurations CShift overcomes the initial expert models and in all, except the PSNR case, the Mean Ensemble.

Implementation and training details. Each graph edge is a neural network with a UNet architecture, as previously validated in NGC [14] and XTC [38]. All 156 graph edges have ≈ 4.3 million parameters, with 4 down-scaling and 4 up-scaling layers and a proper number of input and output channels, depending on the source and destination tasks. We optimize them by jointly minimizing $L2$ and the Structural Similarity Index Measure [34] (SSIM) losses for regression tasks equally-weighted for each neural net. For training edges going to classification tasks (semantic segmentation or halftone), we use Cross-Entropy loss. As optimizer we work with SGD with Nesterov ($\text{lr}=5\text{e-}2$, $\text{wd}=1\text{e-}3$, $\text{momentum}=0.9$), and a ReduceLROnPlateau scheduler ($\text{patience}=10$, $\text{factor}=0.5$, $\text{threshold}=1\text{e-}2$, $\text{min lr}=5\text{e-}5$). Models are trained for 100 epochs during the first iteration, with 9600 training samples. For the second iteration, we perform 100 additional training epochs on both train sets, reaching a total of 19200 training samples. Note that for the second iteration, we train all edges from scratch. For readability, all reported scores in tables are the L1 value $\times 100$.

3.1. Consensus Shift

Ensemble Selection Method. At the core of the selection procedure is the distance function dictating each prediction map’s per-pixel weights, as detailed in Sec. 2.2. In experiments, we instantiate f (Eq. 2) to the weighted median, and for the kernel function K (Eq. 3) we use the identity. We consider different distance metrics, ranging from local per-pixel distances to global perceptual measures, to understand the proposed selection strategy’s power: **1)** L1 and **2)** L2 distances at pixel-level **3)** Peak signal-to-noise ratio (PSNR) to measure the noise of the predictions; **4)** Structure Similarity Index Measure (SSIM) [34] that analyses the luminance, contrast and structural differences; **5)** Learned Perceptual Image Patch Similarity (LPIPS) [43] that is a deep model trained to identify perceptually similar images. We also consider the **6)** per-pixel variance among the multi-path predictions, to

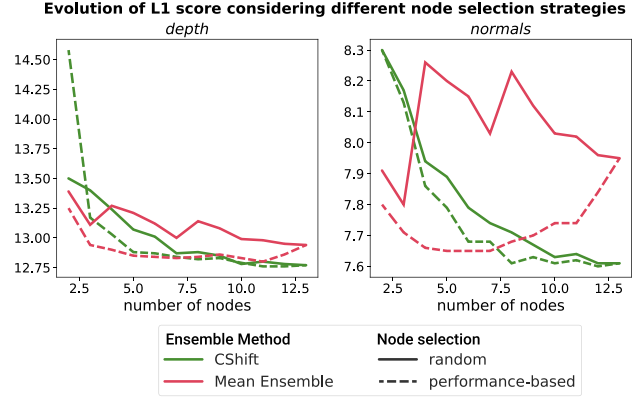


Figure 3. Our selection ensemble is stable under different node selection strategies. It proves its ability to extract relevant information even from low-performing edges, as the performance slightly increases with each new node and its corresponding edge, irrespective of the edge performance. For the mean ensemble, we observe an unstable evolution under the random node selection strategy and a performance decrease when low-performing edges are added to the ensemble in the case of performance-based selection.

quantify their consensus.

In Tab. 2 we present the results of CShift under different selection strategies, for the first iteration. We compare our method against the expert models used to generate the initial pseudo-labels and with a baseline mean ensemble model, which is similar to some extent to [14], as our models are only trained using the expert models while NGC[14] employs a supervised initialization step. Our proposed selection ensemble overcomes the expert models in all the considered configurations while overcoming the simple mean ensemble in all setups except for the PSNR configuration, a combination that is slightly worse for the *normals* task. CShift w/ LPIPS is our top-performing configuration, but all the other metrics prove reliable for the selection ensemble, highlighting its importance in the unsupervised learning process. For all the subsequent experiments, we use CShift w/ LPIPS as our default configuration. Besides *depth* and *normals*, we also report the results for the *rgb* task, measuring the graph model’s ability to reconstruct its original raw input from the ensemble results of its many paths.

Consensus under different sets of nodes. To validate that our model is robust to the set of the considered nodes (and their corresponding in and out edges), we perform an experiment where we start with a small graph containing only two nodes, and, step-by-step, increase the number of nodes until reaching all 13 nodes. The nodes are added to the graph in a specific order. We analyze two ways of establishing this order: 1) random - nodes are randomly sorted; 2) performance-based - nodes are sorted according to their

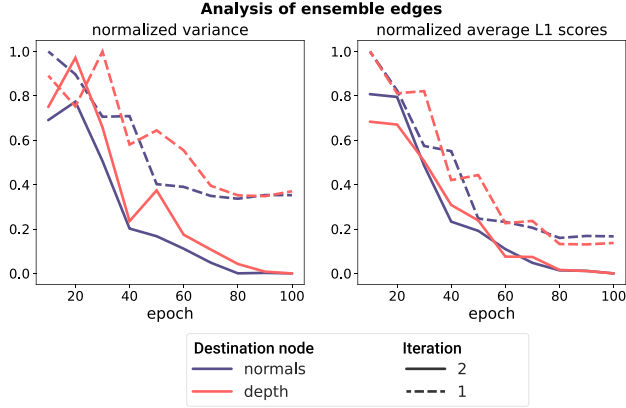


Figure 4. The first plot shows that the average variance over single edges in an ensemble decreases over the training epochs and iterations. Thus, the graph’s average consensus improves from one learning iteration to the next, while the average L1 error of edges decreases (second plot). This proves the CShift approach’s effectiveness and validates that the edges evolve towards the ground truth rather than collapsing in trivial solutions.

individual performance (evaluated w.r.t. to ground truth annotations) and added in this order. In Fig. 3 we present the results of our experiment, comparing CShift with a mean ensemble baseline, for two destination tasks: *depth* and *normals*. In both scenarios, the performance of CShift increases with the number of nodes, proving that our ensemble selection mechanism is able to extract relevant information even from low-performing edges. We significantly overpass the baseline in all configurations. We highlight the performance fluctuations of this baseline that seems to be highly dependent on the performance of the individual edges reaching the ensemble. Our solution is stable even under a random node selection strategy.

Edges improvement between iterations. We give an in-depth analysis of how individual edges evolve over training epochs and CShift iterations. First, in Fig. 4-a, we see how the variance between the edges in an ensemble (reaching *depth* or *normals* task) decreases with more training. This is natural since each edge in the ensemble uses the same pseudo-ground truth annotations. But, in the second iteration, the variance is even smaller, showing a smoother training optimization for the edges (which are trained from scratch for this second iteration). This could be explained by the new pseudo-labels coming from iteration 1 ensembles, rather than experts, making the training process simpler. Next, to validate that the edges do not collapse to a bad representation, we also plot the average L1 error in Fig. 4-b, confirming that all the edges improve their performance towards the ground truth. In Fig. 5 we show those relative improvements per edge, between the two CShift iterations.

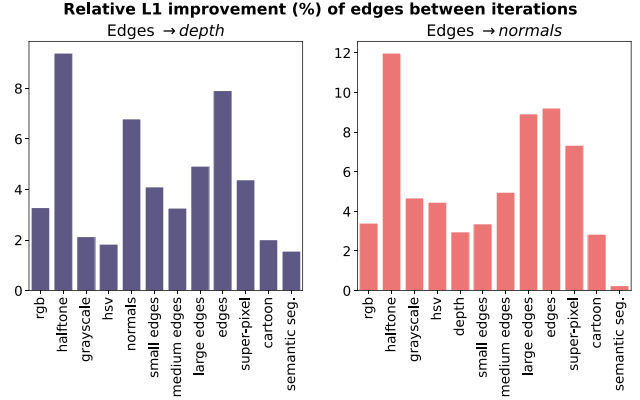


Figure 5. We present the relative performance improvement of the individual edges between iterations. The performance of each edge increases up to almost 12%, proving the capacity of CShift to iteratively adapt to the new domain, in an unsupervised manner.

	<i>rgb</i>	<i>depth</i>	<i>normals</i>
MMD(replica ₁ , replica ₂)	5.4	17.8	17.4
MMD(replica ₁ , hypersim)	3.4	20.1	20.6
MMD(replica ₁ , taskonomy)	13.1	23.3	20.2

Table 3. We report the MMD between our target domain (Replica dataset) and the domains of the *depth* and *normals* expert models (Taskonomy dataset), considering both *rgb* input and mid-level embeddings of the experts. Compared to another synthetic dataset (Hypersim), we observe a smaller distribution shift than for Taskonomy, which contains real-world samples. We also validate our assumptions by comparing two different splits of Replica. For readability, we report $\text{MMD} \times 100$.

3.2. Domain Adaptation

Here we look closer at the gap between the input distribution on which the *depth* and *normals* experts were trained on, and the one for our training and testing dataset, Replica. The experts for these two tasks [38] are trained on the Taskonomy dataset, a real-world dataset. Replica is a synthetic one, and to validate our experiments, we add another synthetic dataset to the comparison: Hypersim [24]. We compute the discrepancy in distribution between Replica and those datasets, using MMD as described in Sec. 2.3. The analysis was performed both for the input level and the expert’s mid-level features. For computing MMD, we average over multiple runs, each containing 100-1600 samples per dataset. The results in Tab. 3 show that there is a significant domain shift in the input for the pre-trained experts on Taskonomy, both at the *rgb* level but also through the eyes of the experts (*depth* and *normals* columns). Notice that the Hypersim dataset is closer to Replica (compared with Taskonomy) since both use synthetic data.

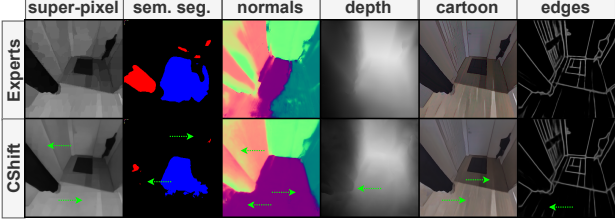


Figure 6. Qualitative results on multiple tasks. On the first row, we show the experts’ output, used as pseudo-labels for training our edges. On the 2nd line we show the output of our CShift. Green arrows point to places where CShift adds significant value in the prediction. From left to right, we see how CShift improves the representation for multiple tasks: super-pixel output has less noise; semantic segmentation removes almost all pixels wrongly classified as ceiling ones; surface normals are significantly corrected; depth catches new details from the curtain; cartoonization output is also less noisy, and on edge detection task it removes some of the noisy edges coming from the floor texture.

		Destination Task (d_{task})		
		<i>depth</i>	<i>normals</i>	<i>rgb</i>
Iter 1	Expert [38]	14.58	8.30	-
	Average of direct edges	14.32	9.34	-
	Edge: $rgb \rightarrow d_{task}$	13.42	8.23	-
	Mean Ensemble [14]	12.94	7.95	4.30
	CShift	12.77	7.61	2.06
Iter 2	Average of direct edges	13.70	8.83	-
	Edge: $rgb \rightarrow d_{task}$	12.98	7.95	-
	Mean Ensemble	12.87	7.91	3.18
	CShift	12.71	7.61	1.51
Improvement over Expert				
Edge: $rgb \rightarrow d_{task}$		11.0%	4.7%	-
CShift ensemble		12.8%	8.3%	-

Table 4. Quantitative results on Replica dataset. We compare our performance over each iteration against the initial experts, on tasks for which we have GT annotations. We outperform XTC experts on *depth* and *normals* by a large margin both with our ensemble, CShift (12.8% and 8.3%), but also with a single Edge (11% and 4.7%), without any additional supervision. With blue we represent the best single edge in the column and with red the best ensemble.

3.3. Experimental Results

Qualitative views for multiple tasks. In Fig. 6, we show the differences between the expert output, used as initial pseudo-ground truth for our graph edges (Fig. 2-a), and the output of our CShift algorithm. Notice that the output of CShift looks smoother and partially corrects the mistakes of the expert model, adding significant value in the output.

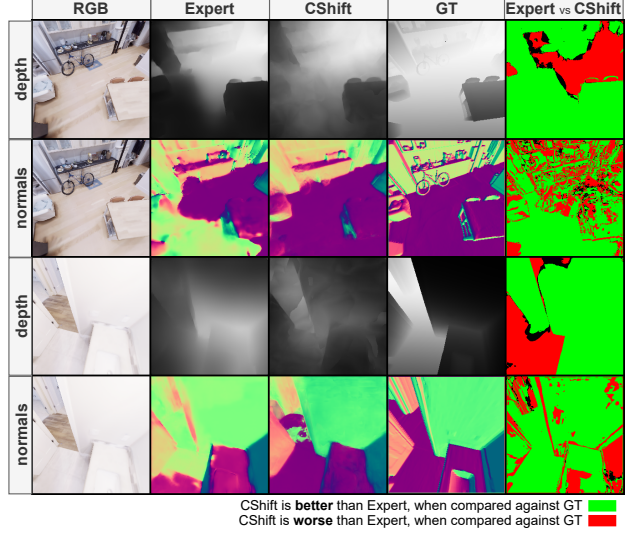


Figure 7. Qualitative results on depth and surface normals, for which we have ground truth annotations. We compare the Expert (col 2) with CShift (col 3). In the last column, we visually show the differences. With green are pixels for which the prediction is improved and with red the ones where the CShift prediction is weaker. On the second line, we see how CShift adds a bike in the scene, where initially in the Expert it is completely missing. This shows that the tasks are interconnected and that CShift takes advantage of their intrinsic links in an unsupervised manner, improving the results not only numerically, but also bringing in new fundamental information extracted from the consensus of all tasks.

Qualitative results for tasks with GT. We compare next in Fig. 7 our results with the Experts, with respect to ground-truth. In the last column, we show with green pixels where CShift outperform the Expert and with red the ones where CShift is weaker. Notice that CShift improves the output at a profound level, bringing in new information in the scene (see the bike in the second row or even the walls in the third). This is due to the multiple different source tasks for the ensembles’ in-edges.

Comparison with other methods. In Tab. 4 we provide a quantitative analysis of our method. Starting from pseudo-labels provided by the experts (*depth* and *normals*), we improve their quality by a large margin both with an ensemble (+12.8% and +8.3%) and with a direct link from *rgb* (+11% and +4.7%). We achieve this performance over two CShift iterations, without adding any supervised information and we also largely outperform the basic mean ensemble. Also, notice that the direct edges in our graph significantly improves over CShift iterations (in average, and individually, the direct edge from *rgb*). Since we treat all tasks unitary, we also train edges with *rgb* as a destination. Interestingly, the *rgb* reconstruction performance improves over iterations.

4. Concluding remarks

We present the consensus shift (CShift) algorithm in multi-task graphs, able to learn unsupervised in novel domains, using as supervision the selective consensus, among the multiple pathways reaching a given task node. The unsupervised capability, fully connected structure, powerful ensemble selection for creating pseudo-labels and then shifting them from one graph learning iteration to the next, make our approach significantly different from related ones. All key aspects of our approach (choice of ensemble selection, multi-task structure, and domain adaptation capabilities) are experimentally validated, while the comparisons to related works prove superior capabilities in the unsupervised learning case. We believe that CShift brings theoretically interesting and practically valuable contributions in an area of research, that of multi-task unsupervised learning, which is of major importance, but not sufficiently studied.

Acknowledgement This work was funded in part by UE-FISCDI, under Projects EEA-RO-2018-0496 and PN-III-P4-ID-PCE-2020-2819.

References

- [1] Pablo Arbelaez, Michael Maire, Charless C. Fowlkes, and Jitendra Malik. Contour detection and hierarchical image segmentation. *IEEE TPAMI*, 2011. 5
- [2] William H. Beluch, Tim Genewein, Andreas Nürnberger, and Jan M. Köhler. The power of ensembles for active learning in image classification. In *CVPR*, 2018. 1
- [3] Mathilde Caron, Ishan Misra, Julien Mairal, Priya Goyal, Piotr Bojanowski, and Armand Joulin. Unsupervised learning of visual features by contrasting cluster assignments. *arxiv*, 2020. 2
- [4] Jeff Donahue and Karen Simonyan. Large scale adversarial representation learning. In *NeurIPS*, 2019. 2
- [5] Matthijs Douze, Arnaud Ramisa, and Cordelia Schmid. Combining attributes and fisher vectors for efficient image retrieval. In *CVPR*, 2011. 2
- [6] Jerome A. Feldman, Gary M. Feldman, Gilbert Falk, Gunnar Grape, J. Pearlman, Irwin Sobel, and Jay M. Tenenbaum. The stanford hand-eye project. In *IJCAI*, 1969. 5
- [7] Spyros Gidaris, Praveer Singh, and Nikos Komodakis. Unsupervised representation learning by predicting image rotations. In *ICLR*, 2018. 2
- [8] Arthur Gretton, Karsten M. Borgwardt, Malte J. Rasch, Bernhard Schölkopf, and Alexander J. Smola. A kernel method for the two-sample-problem. In *NIPS*, 2006. 5
- [9] Joris Guérin and Byron Boots. Improving image clustering with multiple pretrained CNN feature extractors. In *BMVC*, 2018. 1
- [10] Michael Gutmann and Aapo Hyvärinen. Noise-contrastive estimation: A new estimation principle for unnormalized statistical models. In *AISTATS*, 2010. 2
- [11] Tero Karras, Samuli Laine, and Timo Aila. A style-based generator architecture for generative adversarial networks. In *CVPR*, 2019. 5
- [12] Alex Kendall, Yarin Gal, and Roberto Cipolla. Multi-task learning using uncertainty to weigh losses for scene geometry and semantics. In *CVPR*, 2018. 1
- [13] Wouter M. Kouw and Marco Loog. A review of domain adaptation without target labels. *IEEE TPAMI*, 2021. 5
- [14] Marius Leordeanu, Mihai Pirvu, Dragos Costea, Alina Marcu, Emil Slusanschi, and Rahul Sukthankar. Semi-supervised learning for multi-task scene understanding by neural graph consensus. In *AAAI*, 2021. 1, 2, 3, 6, 8
- [15] Yang Liu, Samuel Albanie, Arsha Nagrani, and Andrew Zisserman. Use what you have: Video retrieval using representations from collaborative experts. In *BMVC*, 2019. 1, 2
- [16] Mingsheng Long, Han Zhu, Jianmin Wang, and Michael I. Jordan. Deep transfer learning with joint adaptation networks. In *ICML*, 2017. 5
- [17] Nikolaus Mayer, Eddy Ilg, Philip Häusser, Philipp Fischer, Daniel Cremers, Alexey Dosovitskiy, and Thomas Brox. A large dataset to train convolutional networks for disparity, optical flow, and scene flow estimation. In *CVPR*, 2016. 5
- [18] Antoine Miech, Jean-Baptiste Alayrac, Lucas Smaira, Ivan Laptev, Josef Sivic, and Andrew Zisserman. End-to-end learning of visual representations from uncurated instructional videos. In *CVPR*, 2020. 2
- [19] Antoine Miech, Ivan Laptev, and Josef Sivic. Learning a text-video embedding from incomplete and heterogeneous data. *arxiv*, 2018. 2
- [20] Ishan Misra, C. Lawrence Zitnick, and Martial Hebert. Shuffle and learn: Unsupervised learning using temporal order verification. In *ECCV*, 2016. 2
- [21] Niluthpol Chowdhury Mithun, Juncheng Li, Florian Metze, and Amit K. Roy-Chowdhury. Learning joint embedding with multimodal cues for cross-modal video-text retrieval. In *ICMR*, 2018. 2
- [22] Mandela Patrick, Yuki Markus Asano, Ruth Fong, João F. Henriques, Geoffrey Zweig, and Andrea Vedaldi. Multi-modal self-supervision from generalized data transformations. *arxiv*, 2020. 1, 2
- [23] A. J. Piergiovanni, Anelia Angelova, and Michael S. Ryoo. Evolving losses for unsupervised video representation learning. In *CVPR*, 2020. 1, 2
- [24] Mike Roberts and Nathan Paczan. Hypersim: A photorealistic synthetic dataset for holistic indoor scene understanding. *arXiv* 2020. 7
- [25] Omer Sagi and Lior Rokach. Ensemble learning: A survey. *Data Min. Knowl. Discov.*, 2018. 2
- [26] Xavier Soria, Edgar Riba, and Angel Sappa. Dense extreme inception network: Towards a robust cnn model for edge detection. In *WACV*, 2020. 5
- [27] Xavier Soria, Edgar Riba, and Angel Sappa. Dense extreme inception network: Towards a robust cnn model for edge detection. In *WACV*, 2020. 5
- [28] Julian Straub, Thomas Whelan, Lingni Ma, Yufan Chen, Erik Wijmans, Simon Green, Jakob J. Engel, Raul Mur-Artal, Carl

- Ren, Shobhit Verma, Anton Clarkson, Mingfei Yan, Brian Budge, Yajie Yan, Xiqing Pan, June Yon, Yuyang Zou, Kimberly Leon, Nigel Carter, Jesus Briales, Tyler Gillingham, Elias Mueggler, Luis Pesqueira, Manolis Savva, Dhruv Batra, Hauke M. Strasdat, Renzo De Nardi, Michael Goesele, Steven Lovegrove, and Richard Newcombe. The Replica dataset: A digital replica of indoor spaces. *arXiv*, 2019. 5
- [29] Yonglong Tian, Dilip Krishnan, and Phillip Isola. Contrastive multiview coding. *arxiv*, 2019. 2
- [30] Yonglong Tian, Chen Sun, Ben Poole, Dilip Krishnan, Cordelia Schmid, and Phillip Isola. What makes for good views for contrastive learning. *CoRR*, 2020. 2
- [31] Pavel Tokmakov, Martial Hebert, and Cordelia Schmid. Unsupervised learning of video representations via dense trajectory clustering. *CoRR*, 2020. 2
- [32] Jingdong Wang, Ke Sun, Tianheng Cheng, Borui Jiang, Chaorui Deng, Yang Zhao, Dong Liu, Yadong Mu, Minghui Tan, Xinggang Wang, Wenyu Liu, and Bin Xiao. Deep high-resolution representation learning for visual recognition. *TPAMI*, 2020. 5
- [33] Xinrui Wang and Jinze Yu. Learning to cartoonize using white-box cartoon representations. In *CVPR*, 2020. 5
- [34] Zhou Wang, Alan C Bovik, Hamid R Sheikh, and Eero P Simoncelli. Image quality assessment: from error visibility to structural similarity. *IEEE transactions on image processing*, 13(4):600–612, 2004. 6
- [35] Hongliang Yan, Yukang Ding, Peihua Li, Qilong Wang, Yong Xu, and Wangmeng Zuo. Mind the class weight bias: Weighted maximum mean discrepancy for unsupervised domain adaptation. In *CVPR*, 2017. 5
- [36] Fengting Yang, Qian Sun, Hailin Jin, and Zihan Zhou. Superpixel segmentation with fully convolutional networks. In *CVPR*, 2020. 5
- [37] Meng Ye and Yuhong Guo. Progressive ensemble networks for zero-shot recognition. In *CVPR*, 2019. 1
- [38] Amir Roshan Zamir, Alexander Sax, Nikhil Cheerla, Rohan Suri, Zhangjie Cao, Jitendra Malik, and Leonidas J. Guibas. Robust learning through cross-task consistency. In *CVPR*, 2020. 1, 2, 3, 5, 6, 7, 8
- [39] Amir Roshan Zamir, Alexander Sax, William B. Shen, Leonidas J. Guibas, Jitendra Malik, and Silvio Savarese. Taskonomy: Disentangling task transfer learning. In *CVPR*, 2018. 1, 2, 5
- [40] Xiaohang Zhan, Jiahao Xie, Ziwei Liu, Yew-Soon Ong, and Chen Change Loy. Online deep clustering for unsupervised representation learning. In *CVPR*, 2020. 2
- [41] Richard Zhang, Phillip Isola, and Alexei A. Efros. Colorful image colorization. In *ECCV*, 2016. 2
- [42] Richard Zhang, Phillip Isola, and Alexei A. Efros. Split-brain autoencoders: Unsupervised learning by cross-channel prediction. In *CVPR*, 2017. 2
- [43] Richard Zhang, Phillip Isola, Alexei A Efros, Eli Shechtman, and Oliver Wang. The unreasonable effectiveness of deep features as a perceptual metric. In *Proceedings of the IEEE conference on computer vision and pattern recognition*, pages 586–595, 2018. 6
- [44] Bolei Zhou, Hang Zhao, Xavier Puig, Sanja Fidler, Adela Barriuso, and Antonio Torralba. Scene parsing through ade20k dataset. In *CVPR*, 2017. 5
- [45] Tinghui Zhou, Matthew Brown, Noah Snavely, and David G Lowe. Unsupervised learning of depth and ego-motion from video. In *Proceedings of the IEEE conference on computer vision and pattern recognition*, pages 1851–1858, 2017. 5